Interparticle coulombic decay in coupled quantum dots: Enhanced energy transfer via bridge assisted mechanisms

Hicham Agueny,[1] Maxime Pesche,[2] Bastien Lutet-Toti,[2] Tsveta Miteva,[2] Axel Molle,[2] Jérémie Caillat,[2] and Nicolas Sisourat[2,*]

[1]*Department of Physics and Technology, Allegt. 55, University of Bergen, N-5007 Bergen, Norway*

[2]*Sorbonne Université, CNRS, Laboratoire de Chimie Physique Matière et Rayonnement, UMR 7614, F-75005 Paris, France*

(Received 5 February 2020; revised manuscript received 4 May 2020; accepted 6 May 2020; published 21 May 2020)

Interparticle coulombic decay (ICD) is an efficient energy transfer process between two weakly interacting systems. ICD was recently proposed as the underlying fundamental mechanism for technological purposes based on quantum dot nanostructures, such as wavelength-sensitive detectors. Via ICD, an excited *donor* quantum dot releases its excess energy by ionizing a neighboring *acceptor* dot. Here, we demonstrate that the presence of a third (ICD inactive) quantum dot can serve as a bridge between the two dots, which is shown to result in an enhancement of the efficiency of the ICD-mediated energy transfer. Furthermore, our results show that this enhancement is found to be robust against change in the characteristics of the bridge quantum dot, particularly the depth and size. On the other hand, its relative position with respect to the donor and acceptor dots is found to foster ICD when it is located in between the two dots. Our findings provide new insights for the development of ICD-based nanostructure technologies, particularly for rational design of three coupled quantum dots.

DOI: 10.1103/PhysRevB.101.195431

I. INTRODUCTION

Interparticle coulombic decay (ICD) is an efficient energy transfer process between two weakly interacting systems, first predicted theoretically in [1] and demonstrated experimentally in [2] and [3]. Via ICD, an excited *donor* partner releases its excess energy by ionizing a neighboring *acceptor* species. ICD was demonstrated to be a general phenomenon since the donor and acceptor partners may be ions, atoms, molecules [4–6], quantum wells [7–9], or quantum dots [10–13] (see also [14]). It was also shown that the energy transfer is not restricted to the electronic degrees of freedom and may, for example, involve vibronic couplings when the donor is a vibrationally excited molecule [15].

In terms of applications, it was recently proposed to use ICD in quantum well and quantum dot nanostructures as a fundamental mechanism for technological purposes such as wavelength-sensitive detectors [7,8,12]. However, to achieve a high degree of efficiency of such devices, ICD must be the dominant process. In this context, electron-phonon couplings are the main competing phenomena [16]. In general, the ICD efficiency decreases with increasing distance between the donor and the acceptor partners. In contrast, at a large interparticle distance, electron-phonon couplings are expected to weakly depend on this distance since the nanostructures do not strongly interact with each other [16]. It is therefore essential to determine the optimal interparticle distances that foster the ICD [10] and, thus, permit the enhancement of its efficiency.

In this context, the effects of the shape of quantum dots on the ICD efficiency were investigated, as well as the shape and characteristics of the involved artificial atoms [12,17]. It was also recently shown that another ICD mechanism, so-called superexchange ICD, is possible when the donor and acceptor systems are separated by a bridge atom. For the benchmark neon-helium-neon trimer, it was demonstrated that the ICD between the two neon atoms is substantially enhanced in the presence of a bridge helium atom compared to the isolated neon dimer case [18,19]. In these studies, it was shown that the energy transfer is mediated by virtual states where one electron from one of the neon atoms is transferred to the bridge helium atom.

In the present work, we study numerically the ICD process in coupled quantum dots in order to achieve a high degree of efficiency of the ICD-mediated energy transfer between a donor and an acceptor quantum dot. In particular, we explore the possibility of controlling the ICD by changing the characteristics of the nanostructure. This is achieved using low-dimensional models that effectively model coupled quantum dots, as in [10–13]. The essence of our results is that a clear enhancement of the ICD rate is observed when a third quantum dot is inserted. With the use of a simple physical model based on perturbation theory, we identify the origin of this enhancement and relate it to two physical mechanisms: (i) the bridge dot modifies the continuum states around the resonance, and (ii) it yields additional virtual transitions, which occur via the superexchange ICD mechanism. Moreover, the enhancement is found to exhibit a weak dependence on the parameters of the third quantum dots (i.e., depth and size), which is an interesting finding for rational design of three coupled quantum dots. We further discuss the sensitivity of

*nicolas.sisourat@upmc.fr

the ICD to the location of the third quantum dot with respect to the donor and acceptor dots.

Our investigation of ICD in nanostructures focuses on semiconductors for two and three coupled quantum dots using a one-dimensional (1D) model. Although a 1D model has obvious limitations, our main goal is to search for optimal conditions under which the ICD rate gets enhanced, which is relevant for a full-dimensional model.

Our model as well as its numerical implementation based on the time-dependent Schrödinger equation (TDSE) and perturbation theory is presented in Sec. II. In Sec. III, we report on the ICD efficiency in coupled quantum dot systems with respect to (i) the distance between the donor and the acceptor species and (ii) the characteristics of the bridge quantum dot. The article ends with the conclusions of this work in Sec. IV. Atomic units are used throughout unless stated otherwise.

II. THEORY AND COMPUTATIONAL DETAILS

A. Quantum dot models

We consider 1D models which have proved to properly account for the essential properties of realistic 3D quantum dots with respect to ICD [13]. Such models provide a correct description of the electron dynamics involved in the quantum dots with less computational effort. The effective two-electron Hamiltonian in our systems is given as

$$H(z_1, z_2) = h_1(z_1) + h_2(z_2) + V_C(z_1, z_2), \tag{1}$$

where z_i $(i = 1, 2)$ denotes the coordinate of the ith electron. The one-electron Hamiltonian h_i is of the form

$$h_i(z_i) = -\frac{1}{2}\frac{\partial^2}{\partial z_i^2} + V_{\rm QD}(z_i), \tag{2}$$

where $V_{\rm QD}(z_i)$ is the electron-dot potential (as shown in Fig. 1), built on Gaussian potentials as in [10]

$$V_{\rm QD}(z_i) = -Z_d e^{-\sigma_d(z_i+R/2)^2} - Z_m e^{-\sigma_m(z_i-b_m)^2} - Z_a e^{-\sigma_a(z_i-R/2)^2}. \tag{3}$$

Here, Z_j and σ_j $(j = d, m, a)$ are, respectively, the depth and size of the donor, mediator, and acceptor quantum dot potentials. R is the distance between the donor and the acceptor quantum dots, which are located symmetrically around the origin, and b_m is the coordinate of the mediator center. In this framework, two coupled quantum dots are modeled by setting $Z_m = 0$. In Eq. (1), the single-particle Hamiltonians h_1 and h_2 are coupled via the interaction term $V_C(z_1, z_2)$. The latter is a repulsive soft Coulomb potential and is expressed as

$$V_C(z_1, z_2) = \frac{1}{\sqrt{(z_1 - z_2)^2 + \alpha \exp\left[-\beta(z_1 - z_2)^2\right]}}. \tag{4}$$

This model potential has been chosen to avoid the singularity at $z_1 = z_2$. The same model has been used in previous works to describe the correlated electron-electron interaction in connection with ICD in two coupled quantum dots (see, e.g., [10]).

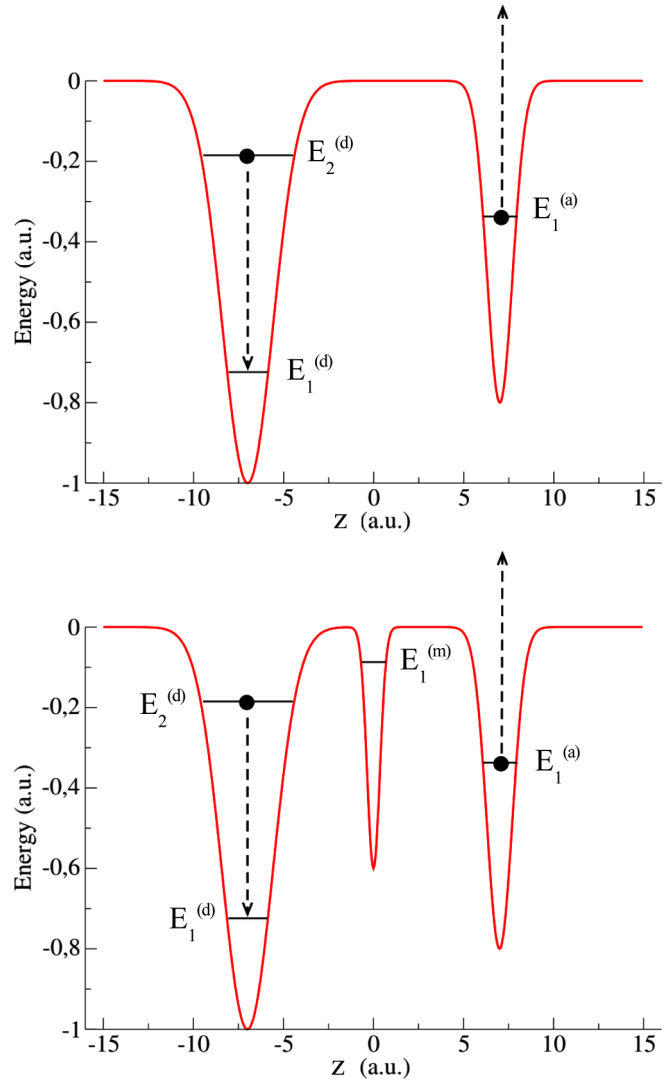

FIG. 1. Schematic of ICD in two (upper panel) and three (lower panel) coupled quantum dots. Via ICD, the left (donor) quantum dot releases its excess energy by ionizing the right (acceptor) dot, as indicated by the arrows. Quantum dots are represented by effective one-dimensional potentials as in [10–13]. $E_n^{(j)}$ denote the one-electron energies (see text).

B. Dynamics and decay widths

The electron dynamics of the nanostructures modeled as above is governed by the TDSE

$$\left[H(z_1, z_2) - i\frac{\partial}{\partial t}\right]\psi(z_1, z_2, t) = 0. \tag{5}$$

We construct the initial wave function from the eigenstates of the one-electron Hamiltonian, in which one electron is localized in the excited state $\phi_2^{(d)}$ of the donor quantum dot and the other in the ground state $\phi_1^{(a)}$ of the acceptor quantum dot:

$$\psi(z_1, z_2, t = 0) = \frac{1}{\sqrt{2}}\left[\phi_2^{(d)}(z_1)\phi_1^{(a)}(z_2) + \phi_2^{(d)}(z_2)\phi_1^{(a)}(z_1)\right]. \tag{6}$$

The energy (E) of the initial state is above the lowest ionization threshold (E_∞) of the two-electron system (i.e., so-called resonant, or quasibound, state). The one-electron states denoted by $\phi_n^{(j)}$ ($j = d, m, a$; $n = 1, 2$) are solutions of the time-independent Schrödinger equation

$$h_i(z_i)\phi_n^{(j)}(z_i) = E_n^{(j)}\phi_n^{(j)}(z_i). \tag{7}$$

The initial wave function is chosen to be symmetric with respect to electron permutation, which corresponds to a singlet spin state. We have also performed the calculations for the triplet-state case. Conclusions similar to those reported below were reached. Note that the symmetry is conserved throughout propagation. At the end of the propagation, the decay width Γ for a given quantum dot system is obtained by fitting the computed values of the autocorrelation function,

$$a(t) = |\langle\psi(t=0)|\psi(t)\rangle|^2, \tag{8}$$

to the generic decay function $e^{-\Gamma t}$.

C. Perturbation model

To help the interpretation of the results stemming from the TDSE, we use a formalism that is reported in [20] and [21]. In our work, the formalism is simplified by making assumptions about the choice of the wave functions involved in the couplings, as shown below (see also [18] and references therein). Here, our main goal is not to obtain quantitatively accurate results for the ICD width as much as to identify and discuss the main contributions that lead to the enhancement of the ICD width in the presence of a third quantum dot. In this context, the decay width is given by

$$\Gamma = 2\pi\,|\langle\psi(t=0)|\hat{H} - E|\psi_f\rangle|^2, \tag{9}$$

where $\psi(t=0)$ and E are the initial state and its energy, respectively [see Eq. (6)]. The final state ψ_f is, in our model,

$$\psi_f = N\left[\psi_k + \frac{\langle\psi_{dm}|\hat{H}|\psi_k\rangle}{(E - E_{dm})}\psi_{dm}\right], \tag{10}$$

where

$$\psi_k = \frac{1}{\sqrt{2}}\left[\phi_1^{(d)}(z_1)k(z_2) + \phi_1^{(d)}(z_2)k(z_1)\right], \tag{11}$$

$$\psi_{dm} = \frac{1}{\sqrt{2}}\left[\phi_2^{(d)}(z_1)\phi_1^{(m)}(z_2) + \phi_2^{(d)}(z_2)\phi_1^{(m)}(z_1)\right], \tag{12}$$

N is a normalization factor, and E_{dm} the energy of the latter state. In Eq. (11), k represents the continuum state at the energy of the ICD electron (i.e., $E - E_\infty$). The second term in Eq. (10) corresponds to the superexchange ICD term in which the energy transfer is mediated by the state where one electron sits in the donor dot while the second electron is in the bridge dot. Note that there are other couplings that could be included in the second term (e.g., one electron is in the ground state of either the donor or the acceptor dot, and the second electron in the bridge). Our calculations, however, show that their contributions are insignificant and thus are omitted from Eq. (10). More details about the evaluation of the decay width using Eq. (10) can be found in [18].

D. Computational details

We used the same parameters to model the donor and acceptor dots as in [10], i.e., $(Z_d, Z_a) = (1.0, 0.8)$ a.u. and $(\sigma_d, \sigma_a) = (0.25, 1.0)$ a.u., while for the mediator quantum dot a broad range of parameters is considered (see below). With the use of these parameters, the donor dot supports two bound states and their eigenenergies are labeled $E_1^{(d)}$ and $E_2^{(d)}$, while the acceptor and mediator dots support only one bound state each and the corresponding energies are labeled $E_1^{(a)}$ and $E_1^{(m)}$, respectively. These single-electron energies are given in Fig. 1 for $R = 14$ a.u. and $b_m = 0$. Note that they do not vary by more than 20% with respect to these parameters in the range of values employed in this work. The time-independent Schrödinger equation [see Eq. (7)] is solved using a Lagrange-mesh method [22,23] with variational basis functions of a sinus form. In the interaction term $V_C(z_1, z_2)$, α and β are soft parameters set to 0.01 and 100 a.u., respectively [10].

The time evolution of the electronic wave function $\psi(z_1, z_2, t)$, which satisfies the TDSE [see Eq. (5)], is solved numerically using a split-operator method combined with a fast Fourier transform algorithm as in [24]. This is carried out on a symmetric 2D grid of size $L = 127.75$ a.u. with the grid spacing $\delta z = 0.25$ a.u., i.e., 512 grid points along each direction. The time step used in the calculation is $\delta t = 0.09$ a.u. The convergence was checked by performing additional calculations with twice the size of the box and a smaller time step. Furthermore, a complex absorbing potential (CAP) placed at positions $\pm z_{\mathrm{CAP}}$ along each coordinate is employed to avoid artificial reflections. It is expressed as [11]

$$W_{\mathrm{CAP}} = -i\eta \mid z_i \pm z_{\mathrm{CAP}} \mid^k \Theta(z \pm z_{\mathrm{CAP}}), \tag{13}$$

where η and k are the strength and the order of the CAP, respectively. Θ is the Heavyside step function. In these calculations, we used $\eta = 0.003$ and $k = 2$. The boundary is chosen such that $z_{\mathrm{CAP}} = \pm 0.85L$. Convergence of the results with respect to the CAP parameters and grid size has been checked.

We applied the fitting procedure to obtain the decay widths [see Eq. (8)] at different final times, ranging from 6200 to 12 400 a.u. The results do not change significantly with respect to the latter values.

III. RESULTS AND DISCUSSION

The ICD mechanisms discussed are schematically depicted in Fig. 1 for the case of two (upper panel) and three (lower panel) coupled quantum dots. The top diagram represents a direct process, in which the excess energy of the donor can be used to directly ionize the electron from the acceptor. In the case of three coupled quantum dots, the excess energy is mediated by the presence of a third quantum dot located between the donor and the acceptor during the ICD. In the perturbation theory picture, this additional effect is taken into account via an extra term related to the superexchange ICD, as outlined in connection with Eq. (10). This mechanism has been discussed for trimers and has been shown to lead to an enhancement of the efficiency of the ICD width [18].

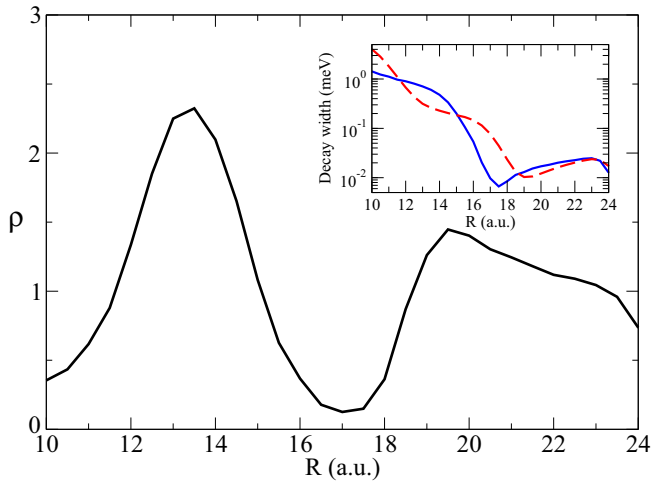

FIG. 2. Ratio between the decay widths for three and two coupled quantum dots as a function of the distance between the donor and the acceptor dots (R). Inset: Decay widths for two (dashed red line) and three (solid blue line) coupled quantum dots. The parameters (see text) of the bridge quantum dot are ($Z_m = 0.6$, $\sigma_m = 4.0$).

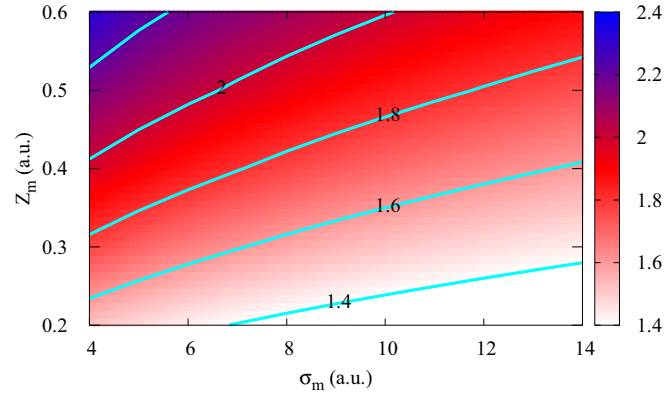

FIG. 3. Ratio between the decay widths for three and two coupled quantum dots as a function of the parameters (see text) of the bridge quantum dot, for $R = 13.5$ a.u. Some contour lines are indicated by the cyan lines.

Stimulated by these recent findings [18] and by fundamental interest in quantum dots for nanotechnological purposes, we aim in this work to search for optimal conditions characterizing a third quantum dot, under which the ICD width gets enhanced. Here the characteristics of this third quantum dot (depth, size, and relative position), which is referred to as the bridge, are chosen such that the energies of the bound states of the donor and acceptor remain unchanged with respect to the case of two coupled quantum dots. This is an important condition for ensuring the physical interpretation of the efficiency of ICD in the presence of a bridge quantum dot.

We consider both scenarios depicted in Fig. 1 and calculate the corresponding decay widths. To evaluate the enhancement of the ICD, we present in Fig. 2 the ratio

$$\rho = \frac{\Gamma_{3\mathrm{QD}}}{\Gamma_{2\mathrm{QD}}} \tag{14}$$

between the decay widths for the three coupled ($\Gamma_{3\mathrm{QD}}$) and two coupled ($\Gamma_{2\mathrm{QD}}$) dots as a function of the distance R between the donor and the acceptor dots (all other parameters fixed). The widths for each system are displayed in the inset in the same figure. The parameters of the bridge quantum dot are $Z_m = 0.6$, $\sigma_m = 4.0$, and $b_m = 0.0$ (i.e., the bridge dot is at the midpoint between the donor and the acceptor dots). It is shown that, in general, the decay widths decrease with increasing R for both systems. However, this trend is not monotonous as already discussed in [10]: for some interparticle distances the electron-electron interaction creates an effective potential that may trap the ICD electron, delaying the decay process (e.g., at $R \simeq 17$ and 19 a.u. for the cases of two and three quantum dots, respectively). The ratio between the decay widths varies between about 0.1 and 2.3, showing that a significantly higher ICD efficiency (i.e., a faster decay) can be achieved for some interparticle distances in the presence of the bridge dot. As shown in the figure, the largest enhancement of the decay process is obtained here at about $R \simeq 13.5$ a.u.

To provide insights into the observed enhancement, we make use of a simple physical model as described in Sec. II C. The model is based on perturbation theory and has the advantage of separating direct processes from indirect ones. The model, therefore, enables us to identify the main contributions responsible for the observed enhancement of the ICD width in Fig. 2. Here, the bridge quantum dot can lead to the observed enhancement around $R \simeq 13.5$ a.u. via two mechanisms: it can modify the continuum states around the resonance (see [7] for more details) and can participate in the energy transfer via superexchange ICD. To disentangle and quantify both contributions we have computed the decay widths using the perturbation model reported in Sec. II C. Above $R = 12$ a.u., the result stemming from this model agrees quantitatively with that of the numerically exact TDSE calculations. Below $R = 12$ a.u., the coupling between ψ_k and ψ_{dm} becomes too strong and the perturbation correction is not adequate. We, therefore, focus on the results of the model within its range of validity (i.e., $R > 12$ a.u.). By removing the superexchange ICD term in Eq. (10) (i.e., $\psi_f = \psi_k$), it is possible to quantify the contributions of both mechanisms discussed above. These calculations show that both mechanisms contribute nearly equally for $R \sim 13.0$-18.0 a.u. (not shown). At larger distances, the superexchange ICD mechanism does not contribute since the coupling between ψ_{dm} and ψ_k decreases exponentially with the distance (see [18]). We mention here that the perturbation model predicts that the superexchange ICD mechanism largely dominates at distances below 12.0–13.0 a.u. However, as noted above the model is not quantitative in this interparticle distance range and further work is needed.

We now investigate the sensitivity of ICD with respect to the parameters of the bridge species. In Fig. 3, we present the ratio ρ [Eq. (14)] as a function of Z_m and σ_m. The distance between the donor and the acceptor species is fixed at $R = 13.5$ a.u. and b_m is kept equal to 0 (i.e., the bridge dot is again fixed at the midpoint between the donor and the acceptor dots). Our results show that, for Z_m ranging from 0.3 to 0.6 and

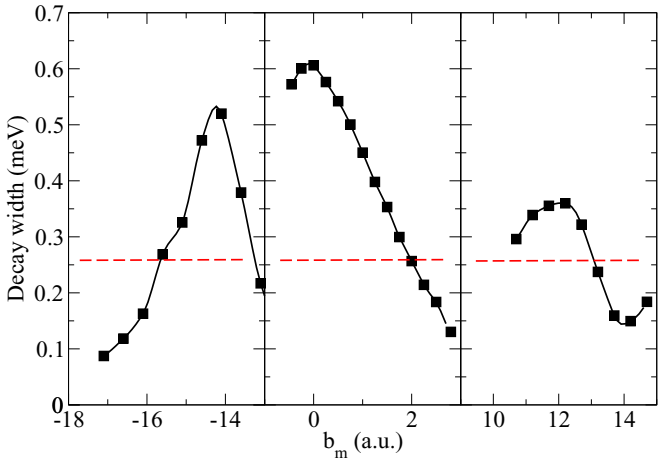

FIG. 4. Decay widths as a function of the position of the bridge quantum dot, for $R = 13.5$ a.u. (i.e., the donor and acceptor dots are fixed at -6.75 and 6.75 a.u., respectively.). The dashed red line indicates the decay width in the absence of the bridge. Note that we have limited the range of b_m to values that do not change significantly the energies of the donor and acceptor dots with respect to the case of two coupled quantum dots.

σ_m ranging from 4 to 10 a.u., the ICD width is enhanced in the presence of the bridge dot by a factor of between about 1.6 and 2.4.

Furthermore, in Fig. 4, we show the decay width as a function of the position b_m of the bridge quantum dot, for $R = 13.5$ a.u. We report only results for values of b_m which do not modify significantly the energies of the donor and acceptor quantum dots, compared to the centered case ($b_m = 0$). One can see in the middle panel that the enhancement of the ICD process is maximal when the bridge dot is at the midpoint between the other two quantum dots. The ICD process becomes weaker as the bridge dot approaches the acceptor dot (i.e., $b_m > 0$). The energies of the donor are significantly modified when the bridge dot is moved towards it (i.e., $b_m < 0$). A change in the donor potential affects the efficiency of the ICD process. As mentioned above, we are interested in the enhancement of the ICD process owing only to the presence of the third dot. We therefore do not report results for $-13 < b_m < 0$.

The left and right panels in Fig. 4 show the decay width when the bridge dot is located on the left side of the donor ($b_m < -R/2$) or on the right side of the acceptor ($b_m > +R/2$), respectively. It is interesting to note that the ICD is substantially enhanced when the bridge dot is placed on the left side of the donor dot, showing that the relative position of the bridge, donor, and acceptor dots is also a relevant parameter for optimization of the ICD rate. The observed behavior of the decay widths, reported in Fig. 4, is related to interferences between the direct path [i.e., $\psi(t = 0) \rightarrow \psi_k$] and the one corresponding to the transition via the virtual state ψ_{dm} (i.e., via the superexchange ICD mechanism). These interferences lead to the enhancement or suppression of the decay width depending on the location of the bridge quantum dot. This can be understood from the perturbation model defined above, which incorporates virtual transitions in the final state, as shown in Eq. (10). A similar effect has recently been discussed for three-body ICD processes occurring in atomic clusters [25].

At this point, we conclude that efficiency of the ICD-mediated energy transfer can be achieved for a broad range of parameters characterizing the inserted bridge quantum dot. This is an interesting finding for rational design of three coupled quantum dots.

IV. CONCLUSION

We have shown that energy transfer mediated by the interparticle coulombic decay process between two quantum dots can be substantially enhanced in the presence of a third bridge dot. The efficiency of the process can thus be improved by more than a factor of 2. Furthermore, we have investigated the mechanisms leading to this increase and how the latter depends on the characteristics (depth, size, and relative position) of the bridge species. It was found that the efficiency of the ICD is robust against change of the depth and size of the inserting bridge dot. On the other hand, this efficiency was shown to be sensitive to the relative position of the bridge dot with respect to the donor and acceptor quantum dots. Our findings, therefore, offer alternative routes to manipulate ICD and ultimately design three coupled quantum dots. This work provides new insights into the energy transfer processes in nanostructures and should be useful for the development of quantum-dot-based technologies.

ACKNOWLEDGMENTS

This project received funding from the LabEx MiChem part of French state funds managed by the ANR within the Investissements d'Avenir program under the reference ANR-11-IDEX-0004-02. Computations were performed on resources provided by UNINETT Sigma2—the National Infrastructure for High Performance Computing and Data Storage in Norway.

[1] L. S. Cederbaum, J. Zobeley, and F. Tarantelli, Phys. Rev. Lett. **79**, 4778 (1997).

[2] S. Marburger, O. Kugeler, U. Hergenhahn, and T. Möller, Phys. Rev. Lett. **90**, 203401 (2003).

[3] T. Jahnke, A. Czasch, M. S. Schöffler, S. Schössler, A. Knapp, M. Käsz, J. Titze, C. Wimmer, K. Kreidi, R. E. Grisenti, A. Staudte, O. Jagutzki, U. Hergenhahn, H. Schmidt-Böcking, and R. Dörner, Phys. Rev. Lett. **93**, 163401 (2004).

[4] V. Averbukh, P. V. Demekhin, P. Kolorenč, S. Scheit, S. D. Stoychev, A. I. Kuleff, Y.-C. Chiang, K. Gokhberg, S. Kopelke, N. Sisourat, and L. S. Cederbaum, J. Electron Spectrosc. Relat. Phenom. **183**, 36 (2011).

[5] U. Hergenhahn, J. Electron Spectrosc. Relat. Phenom. **184**, 78 (2011).

[6] T. Jahnke, J. Phys. B: At. Mol. Opt. Phys. **48**, 082001 (2015).

[7] T. Goldzak, L. Gantz, I. Gilary, G. Bahir, and N. Moiseyev, Phys. Rev. B **91**, 165312 (2015).
[8] T. Goldzak, L. Gantz, I. Gilary, G. Bahir, and N. Moiseyev, Phys. Rev. B **93**, 045310 (2016).
[9] T. Goldzak, Mol. Phys. **117**, 2179 (2019).
[10] A. Bande, K. Gokhberg, and L. S. Cederbaum, J. Chem. Phys. **135**, 144112 (2011).
[11] F. M. Pont, A. Bande, and L. S. Cederbaum, Phys. Rev. B **88**, 241304(R) (2013).
[12] P. Dolbundalchok, D. Pelez, E. F. Aziz, and A. Bande, J. Comp. Chem. **37**, 2249 (2016).
[13] F. M. Pont, A. Bande, and L. S. Cederbaum, J. Phys.: Condens. Matter **28**, 075301 (2016).
[14] See http://www.pci.uni-heidelberg.de/tc/usr/icd/ICD.refbase.html for the complete list of ICD papers.
[15] L. S. Cederbaum, Phys. Rev. Lett. **121**, 223001 (2018).
[16] A. Bande, Mol. Phys. **117**, 2014 (2019).
[17] F. Weber, E. F. Aziz, and A. Bande, J. Comput. Chem. **38**, 2141 (2017).
[18] T. Miteva, S. Kazandjian, P. Kolorenč, P. Votavová, and N. Sisourat, Phys. Rev. Lett. **119**, 083403 (2017).
[19] P. Votavová, T. Miteva, S. Engin, S. Kazandjian, P. Kolorenč, and N. Sisourat, Phys. Rev. A **100**, 022706 (2019).
[20] U. Fano, Phys. Rev. **124**, 1866 (1961).
[21] G. Howat, T. Åberg, and O. Goscinski, J. Phys. B At. Mol. Opt. Phys. **11**, 1575 (1978).
[22] D. Baye and P. H. Heenen, J. Phys. A: Math. Gen. **19**, 2041 (1986).
[23] H. Agueny, A. Makhoute, A. Dubois, and J. P. Hansen, Phys. Rev. A **93**, 012713 (2016).
[24] H. Agueny and J. P. Hansen, Phys. Rev. A **98**, 023414 (2018).
[25] R. Bennett, P. Votavová, P. Kolorenč, T. Miteva, N. Sisourat, and S. Y. Buhmann, Phys. Rev. Lett. **122**, 153401 (2019).